Hindawi Publishing Corporation
Active and Passive Electronic Components
Volume 2016, Article ID 4027406, 11 pages
http://dx.doi.org/10.1155/2016/4027406

Research Article

Considerations of Physical Design and Implementation for 5 MHz-100 W LLC Resonant DC-DC Converters

Akinori Hariya,[1] Ken Matsuura,[2] Hiroshige Yanagi,[3] Satoshi Tomioka,[3] Yoichi Ishizuka,[1] and Tamotsu Ninomiya[4]

[1]*Nagasaki University, Graduate School of Engineering, 1-14 Bunkyo-machi, Nagasaki-shi, Nagasaki, Japan*
[2]*TDK Corporation, 2-15-7 Higashiowada, Ichikawa-shi, Chiba, Japan*
[3]*TDK-Lambda Corporation, 2704-1 Settaya, Nagaoka-shi, Nigata, Japan*
[4]*Green Electronics Research Institute, Kitakyushu, 1-1 Jyonai, Kokurakita-ku, Kitakyushu-shi, Fukuoka, Japan*

Correspondence should be addressed to Akinori Hariya; bb52312202@ms.nagasaki-u.ac.jp

Received 3 June 2016; Accepted 29 August 2016

Academic Editor: Hongyang Zhao

Recently, high power-density, high power-efficiency, and wide regulation range isolated DC-DC converters have been required. This paper presents considerations of physical design and implementation for wide regulation range MHz-level LLC resonant DC-DC converters. The circuit parameters are designed with 3–5 MHz-level switching frequency. Also, the physical parameters and the size of the planar transformer are optimized by using derived equations and finite element method (FEM) with Maxwell 3D. Some experiments are done with prototype LLC resonant DC-DC converter using gallium nitride high electron mobility transistors (GaN-HEMTs); the input voltage is 42–53 V, the reference output voltage is 12 V, the load current is 8 A, the maximum switching frequency is about 5 MHz, the total volume of the circuit is 4.1 cm^3, and the power density of the prototype converter is 24.4 W/cc.

1. Introduction

Recently, high power-density and high power-efficiency isolated DC-DC converters have been required in information and communication technology (ICT) facilities. Therefore, high switching frequency and low power loss technique have been studied. In particular, to achieve these requirements, the isolated DC-DC converters with GaN-HEMTs have been studied by some research institute in recent years [1–7].

Furthermore, the regulated MHz-level operated isolated DC-DC converters have been studied with wide input voltage: 60–120 V input voltage, 20 V output voltage, 2.6 MHz switching frequency, and 50 W output power, series resonant DC-DC converter [8]; 36–72 V input voltage, 12 V output voltage, 5 MHz switching frequency, and 30 W output power, flyback DC-DC converter [9]; 110–250 V input voltage, 15 V output voltage, 2 MHz switching frequency, and 45 W output power, quasi-square-wave zero-voltage switching three-level half-bridge DC-DC converter [10]; 60–120 V input voltage, 15 V output voltage, 3–4.5 MHz switching frequency, and 40 W output power, zero-voltage switching (ZVS) half-bridge DC-DC converter [11]. These isolated DC-DC converters achieve high power efficiency. However, higher power efficiency and higher output power are required in MHz-level frequency isolated DC-DC converter.

LLC resonant DC-DC converters have been known to achieve high power efficiency with high switching frequency. In case of this topology, the regulated converters of 1 MHz-level switching frequency have been studied so far [12, 13]. Also, the unregulated LLC resonant DC-DC converters operated at 5 MHz have been considered so far [14]. In order to achieve the miniaturization of the converter, LLC resonant DC-DC converters with wide input voltage and high power efficiency are needed at higher switching frequency.

In this paper, the designs of high power-density and wide regulated LLC resonant DC-DC converter have been considered. The circuit parameters have been calculated for wider regulation at MHz-level switching frequency. The target input

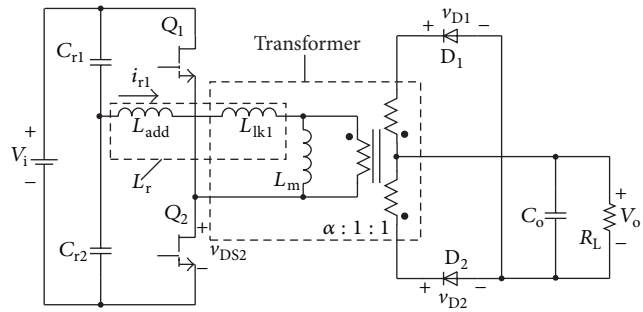

Figure 1: LLC resonant DC-DC converter circuit topology.

Table 1: The target specification of the prototype DC-DC converter.

Input voltage range: V_i	42–53 V (48 V)
Reference output voltage: V_o	12 V
Output power: P_o	100 W
Power efficiency: η	More than 90%
Volume	3.3 cm^3
Power density	30 W/cc

voltage is 42–53 V, output voltage is 12 V, output power is 100 W, and power efficiency is more than 90%. This design procedure includes planar transformer design with FEM of Maxwell 3D. To evaluate the performance of the prototype board, the experiment has been conducted with open loop.

In Section 2, the consideration of LLC resonant DC-DC converter circuit parameter is described. In Section 3, the physical design considerations of planar transformer are revealed. In Section 4, the experimental results are demonstrated.

2. The Consideration of Circuit Parameter Design

The circuit topology is based on a LLC resonant DC-DC converter, as shown in Figure 1. The target specification is shown in Table 1. The primary side is a half-bridge topology. Q_1 and Q_2 are driven in 50% duty ratio, alternatively. C_{r1} and C_{r2} are the resonant capacitances which have the same capacitance. Also, they make averaged voltage of C_{r2} to one half of the input. The magnetic transformer is composed of leakage inductance L_{lk1} and magnetizing inductance L_m. L_{add} is primary-side additional inductance. The secondary side is the center-tap topology with diodes D_1 and D_2. To achieve target input voltage range, transformer turn ratio is set to be 3.

LLC resonant DC-DC converters have two resonant frequencies. One is the series resonant frequency f_0 which is series resonance between resonant capacitance C_r and inductance L_r. The other is the resonant frequency f_1 which is resonance between C_r, L_r and magnetizing inductance L_m. LLC resonant DC-DC converter can operate in the region of

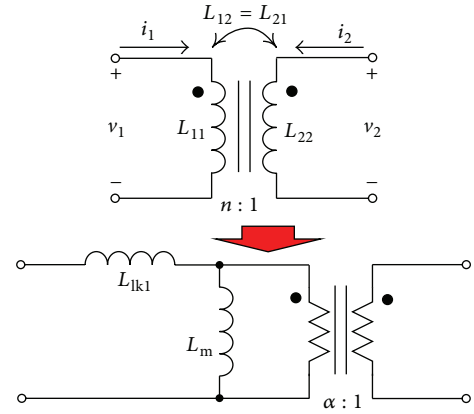

Figure 2: The equivalent circuit of the magnetic transformer.

above resonance $f_s > f_0$ or below resonance $f_1 < f_s < f_0$. In case of above resonance, ZVS of primary-side switches can be achieved. In this region, the converter behaves as buck-mode operation. In case of below resonance, ZVS of primary-side switches and zero-current switching (ZCS) of secondary-side diodes can be achieved. In this region, the converter behaves as boost-mode operation. LLC resonant DC-DC converter used in this paper is operated in below resonance at rated current.

In order to achieve the target specification, the design of LLC resonant DC-DC converter is considered. At first, the equivalent circuit of the magnetic transformer can be drawn, as shown in Figure 2 [15]. Also, the following equations can be obtained:

$$L_{lk1} = \left(1 - k^2\right) L_{11},$$
$$L_m = k^2 L_{11},$$
$$\alpha = kn = k\sqrt{\frac{L_{11}}{L_{22}}}, \tag{1}$$

where L_{lk1} is the leakage inductance, L_m is the magnetizing inductance, k is the coupling coefficient, L_{11} is the primary-side self-inductance, L_{22} is the secondary-side self-inductance, and n is the turn ratio.

In LLC resonant DC-DC converter, for achieving ZVS operation of primary-side switches, the magnetizing inductance has to be designed small enough. The magnetizing inductance can result in the following equation [16, 17]:

$$L_m \leq \frac{T_s t_{dead}}{16 C_{oss}}, \tag{2}$$

where T_s is the switching period, t_{dead} is the dead time of the primary-side switches, and C_{oss} is the output capacitance of the primary-side switches. From this equation, when the parameters are set as $T_s = 250$ ns, $t_{dead} = 10$ ns, and $C_{oss} = 654$ pF at $V_i = 42$ V, the value of $L_m < 238.9$ nH can be derived. Therefore, the magnetizing inductance can be set at 220 nH. Also, LLC resonant DC-DC converter has been analyzed with fundamental harmonic approximation (FHA) [16, 17]. The definitions for this analysis are as follows:

$$\omega_s = 2\pi f_s, \tag{3}$$

$$\omega_0 = 2\pi f_0 = \frac{1}{\sqrt{L_r C_r}}, \tag{4}$$

$$F = \frac{f_s}{f_0} = \frac{\omega_s}{\omega_0}, \tag{5}$$

$$Q = \frac{Z_0}{R_{ac}} = \frac{1}{R_{ac}}\sqrt{\frac{L_r}{C_r}}, \tag{6}$$

$$L_{11} = L_{lk1} + L_m, \tag{7}$$

$$L_r = L_{add} + L_{lk1}, \tag{8}$$

$$K = \frac{L_m}{L_r}, \tag{9}$$

$$C_r = C_{r1} + C_{r2}, \tag{10}$$

$$R_{ac} = \frac{8}{\pi^2} R_L, \tag{11}$$

where f_s is the switching frequency, f_0 is the resonant frequency, Q is the quality factor of the circuit, R_{ac} is the equivalent resistance, C_r is the resonant capacitance, L_r is the resonant inductance, L_{add} is the additional inductance for optimizing L_r, and K is the ratio of the inductances. The equivalent circuit of LLC resonant DC-DC converter can be drawn, as shown in Figure 3. From this equivalent circuit, the ratio of the input and output voltage M can be obtained as follows:

$$M = \frac{v_{ac}}{v_s} = \frac{2\alpha V_o}{V_i} = \frac{1}{\sqrt{\left(1 + (1/K)\left(1 - 1/F^2\right)\right)^2 + Q^2\left(F - 1/F\right)^2}}. \tag{12}$$

When k is set to 0.94, α is decided at 2.82. The minimum input voltage is 42 V; thus, the required peak ratio M_p can be

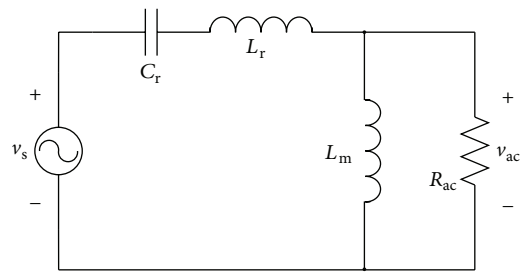

Figure 3: The equivalent circuit of LLC resonant DC-DC converter in FHA.

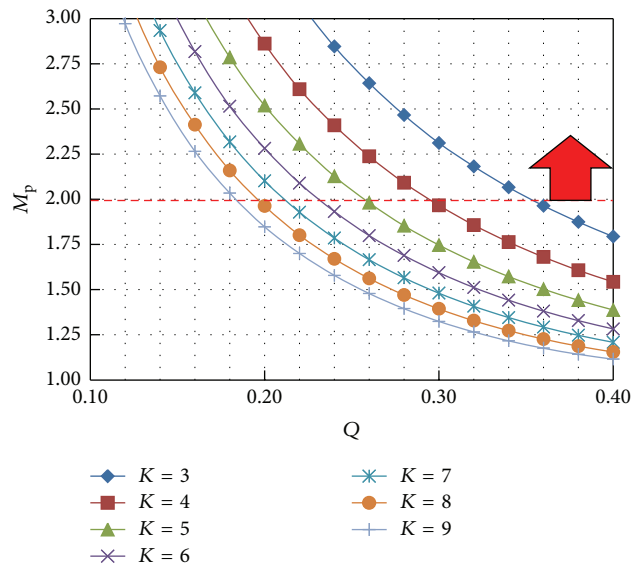

Figure 4: The relationship between peak ratio M_p and the quality factor Q.

derived about 2 from (12). This result includes 20% margin of M. Figure 4 can result from (12). The limitation of Q in each K can be found from this graph. B82801B manufactured by EPCOS is used as not only current measurement but also additional inductance. The short inductance of the current transformer is 7 nH. Therefore, from Figure 5, when $K = 6$, L_r is decided about 36.7 nH. Also, from Figure 4, $Q < 0.23$. Then, C_r and f_0 can be decided from (6) and (4), respectively; $C_r = 12.66$ nF and $f_0 = 7.4$ MHz.

3. The Physical Design Considerations of Planar Transformer

In general, Nickel Zinc (NiZn) ferrite core has been used in MHz-level switching frequency operation. In terms of the core of this prototype isolated DC-DC converter, SY22 NiZn ferrite core manufactured by TDK is used [18]. The relative permeability μ_i of the core material is 80. This core material can be used from 5 to 15 MHz. The good features are guaranteed in MHz-level frequency. The core shape is EI

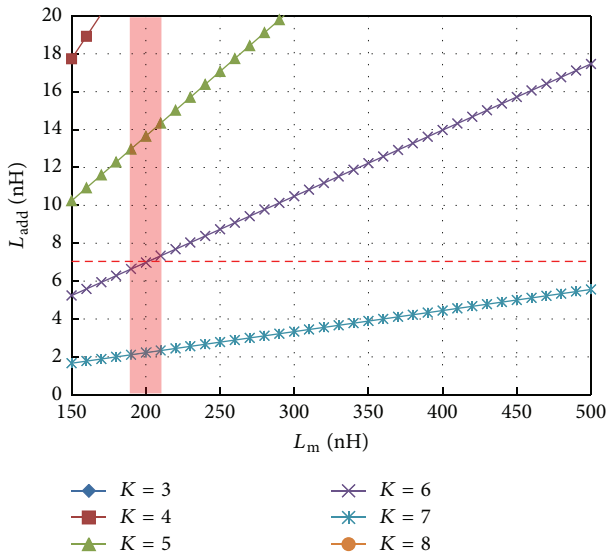

FIGURE 5: The relationship between the magnetizing inductance L_m and the additional inductance L_{add}.

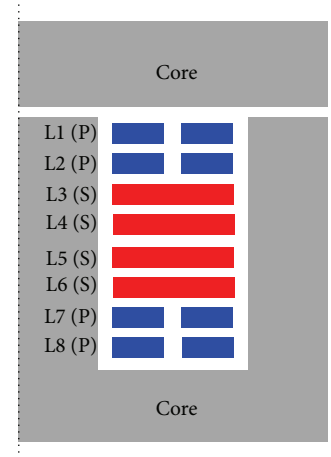

FIGURE 6: The winding arrangement of the prototype planar transformer.

core. In this paper, the physical parameters of this EI core are optimized for obtaining good performance.

For the prototype LLC resonant DC-DC converter, 8-layer printed circuit board (PCB) is used. The winding arrangement of the prototype planar transformer is shown in Figure 6. In terms of planar transformer, layers 1, 2, 7, and 8 (L1, 2, 7, and 8) are assigned to primary-side windings, while layers 3, 4, 5, and 6 (L3, 4, 5, and 6) are assigned to secondary-side windings. The primary-side turn number is 3 turns, 1 layer has 2 turns, and parallel number is 2. Also, the secondary-side turn number is 1 turn, 1 layer has 1 turn, and parallel number is 2. Each diode is connected with each secondary-side winding, as shown in Figure 1.

Figure 7 shows the definitions for each physical parameter of magnetic transformer which have EI core. From these definitions, the following equation can be obtained:

$$\begin{aligned} w_2 &= 2w_1 + g, \\ p &= w_2 + 2g, \\ b &= \frac{l_e}{2} - h - p, \\ c &= 2(b + p), \\ V_e &= ab \cdot 2(b + p + h) = A_e l_e, \end{aligned} \tag{13}$$

where l_e is effective magnetic path length, A_e is effective core cross-sectional area, and V_e is volume of core material. In addition, based on magnetic circuit of EI core transformer, the following equation can be derived:

$$A_e = \frac{\left(C_c L_{11}\left(2\mu_s l_g + l_e\right)\right)}{\left(\mu_0 \mu_s {N_p}^2\right)}, \tag{14}$$

where C_c is correction coefficient, μ_0 is absolute permeability, l_g is air gap, μ_s is relative permeability of core material, and N_p is number of primary-side turns.

The restriction of this converter is considered. The physical features of each component are shown in Figure 8. Target depth, width, height, and volume are written in this figure. From these physical features, the limitation of physical parameters in magnetic transformer can be derived as follows: $0 < a < 15 - 2p$ and $c \leq 16.5$.

The relationship between B_m and temperature can be drawn from past experimental data, as shown in Figure 9. B_m can be derived as the following equation from experimental results:

$$B_m = \frac{(v_m t_m)}{\left(2N_p A_e\right)}. \tag{15}$$

From this data, when the allowable temperature of magnetic core is set to 80°C, B_m is restricted from 32 to 36 mT.

From Figures 10(a) and 10(b), the length of the winding in the primary-side and secondary-side can be calculated as follows:

$$\begin{aligned} l_p &= 4a + 3.5b + 15w_1 + 21.5g, \\ l_s &= 2a + b + 8w_2 + 8g. \end{aligned} \tag{16}$$

Each layer of resistance is shown here:

$$\begin{aligned} R_{lay\_i} &= r_{lay\_i} l_p, \\ R_{lay\_j} &= r_{lay\_j} l_s, \end{aligned} \tag{17}$$

where $i = 1, 2, 7, 8$ and $j = 3, 4, 5, 6$. Also, r_{lay_i} and r_{lay_j} are winding resistance per unit length. The winding resistance per unit length r_{lay} is obtained from simplified Maxwell 3D winding model, as shown in Figure 11. The solver of the simulation is eddy current. The thickness of L1 and L8 is 0.073 mm, that of L2 and L7 is 0.055 mm, and that of L3–6 is

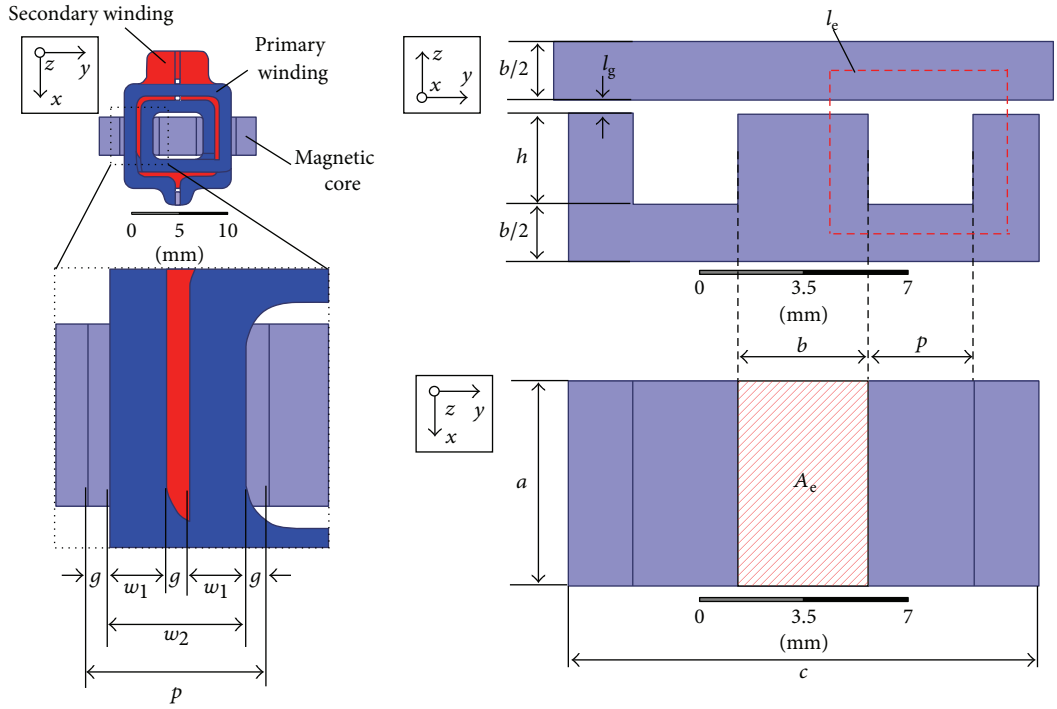

FIGURE 7: The definitions for each physical parameter of magnetic transformer.

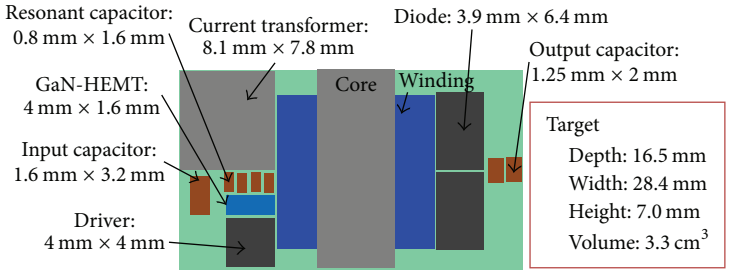

FIGURE 8: The physical features of each component.

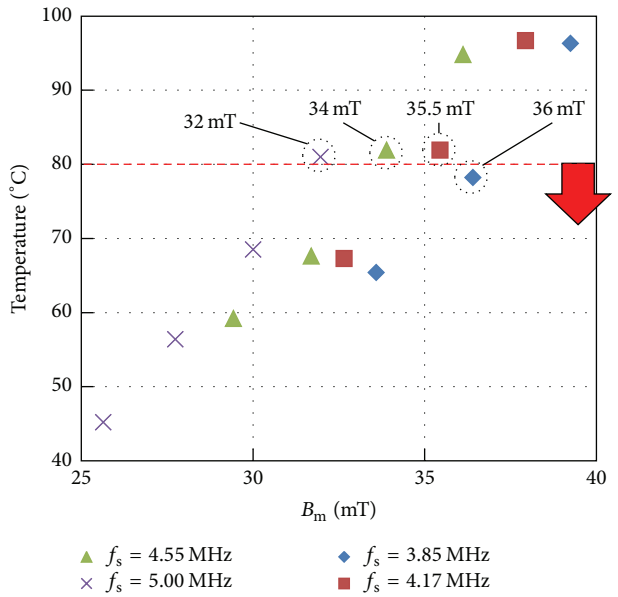

FIGURE 9: B_m versus temperature derived by past experimental data (core: SY22, N_p = 2 turns, V_e = 1159.62 mm^3, A_e = 30.8 mm^2, and l_g = 0.5 mm).

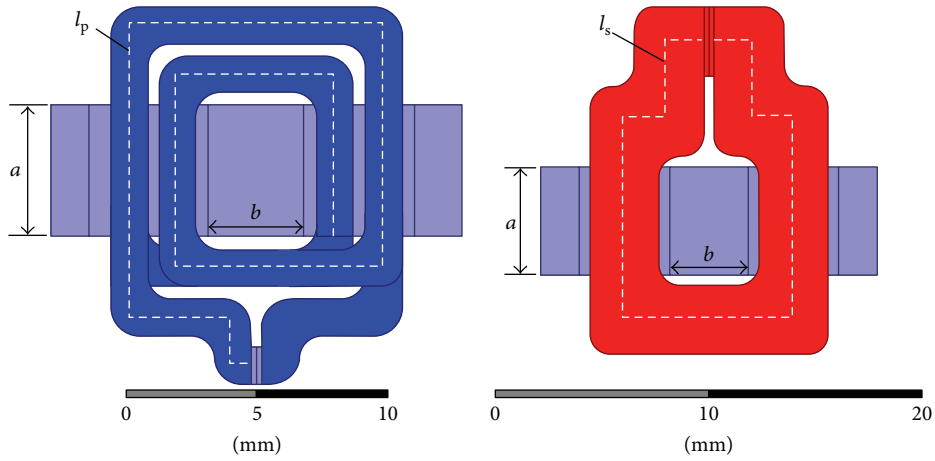

(a) The primary-side length (b) The secondary-side length

FIGURE 10: The length of the winding.

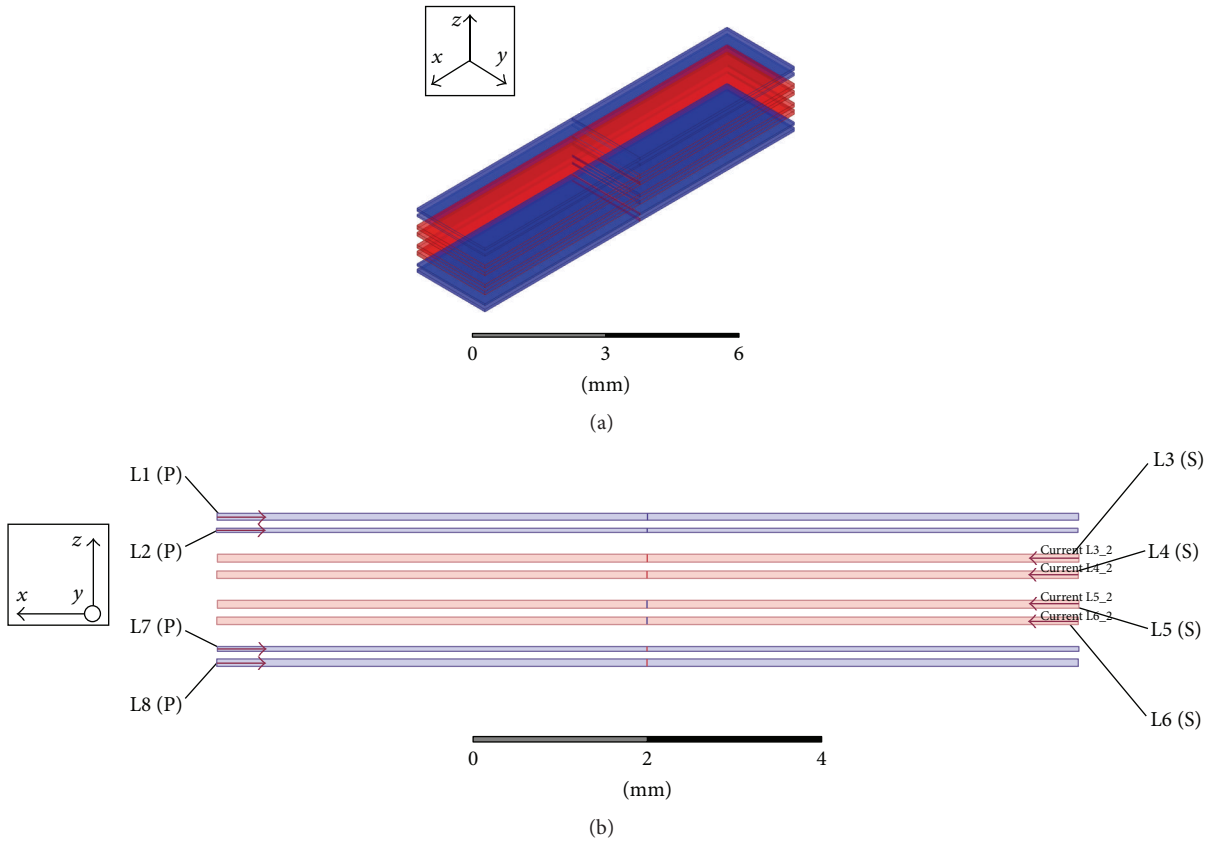

FIGURE 11: Simplified Maxwell 3D winding model.

0.090 mm. These thicknesses are the real copper foil thickness of PCB board. Also, each material is copper where bulk conductivity is 46×10^6 S/m. The frequency of the simulation is 5 MHz. The current direction of this simulation is shown in Figure 11(b). The results of the simulation are shown in Figure 12. These results indicate the relationship between the winding width w and the winding resistance per unit length r_{lay}. From the approximate of the plot, the relationship equation can be obtained as follows:

$$\begin{aligned} r_{\text{lay }1,8} &= 0.7047w^{-0.605}, \\ r_{\text{lay }2,7} &= 0.9195w^{-0.667}, \\ r_{\text{lay }3,4,5,6} &= 0.8040w^{-0.635}. \end{aligned} \tag{18}$$

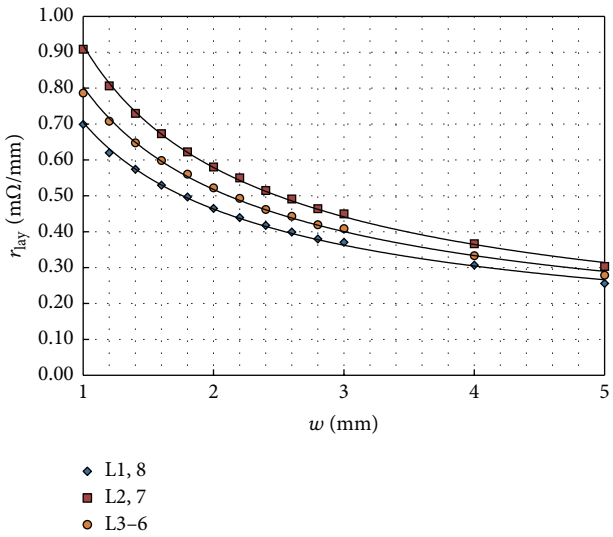

FIGURE 12: The results of the simulation: the relationship between the winding width w and the winding resistance per unit length r_{lay}.

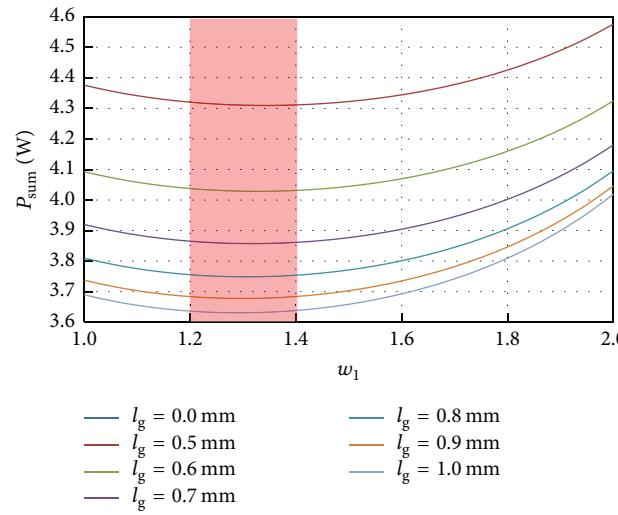

FIGURE 13: w_1 versus P_{sum} (fixed parameters: L_{11} = 250 nH, μ_s = 80, N_p = 3, $\mu_0 = 4\pi \times 10^{-7}$ H/m, h = 2 mm, and g = 0.5 mm).

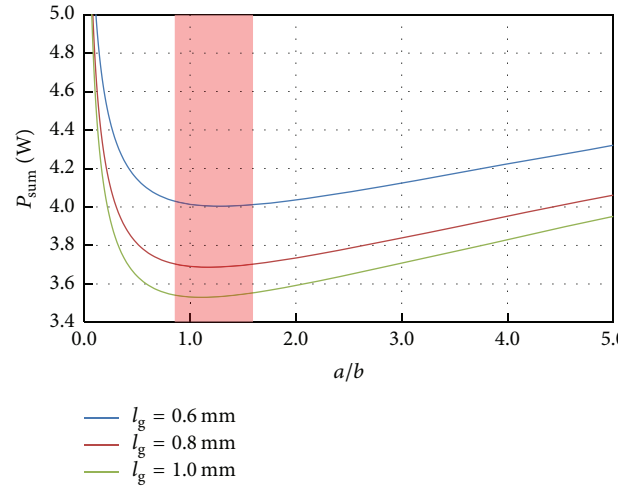

FIGURE 14: a/b versus P_{sum} (fixed parameters: L_{11} = 250 nH, μ_s = 80, N_p = 3, $\mu_0 = 4\pi \times 10^{-7}$ H/m, h = 2 mm, and g = 0.5 mm).

As mentioned above, layers 1, 2, 7, and 8 are assigned to primary-side windings, while layers 3, 4, 5, and 6 are assigned to secondary-side windings. The primary-side turn number is 3 turns, 1 layer has 2 turns, and parallel number is 2. Also, the secondary-side turn number is 1 turn, 1 layer has 1 turn, and parallel number is 2. Thus, each winding resistance is

$$R_{pri} = \frac{\left(R_{lay\,1} + R_{lay\,2}\right)\left(R_{lay\,7} + R_{lay\,8}\right)}{\left(R_{lay\,1} + R_{lay\,2}\right) + \left(R_{lay\,7} + R_{lay\,8}\right)},$$
$$R_{sec} = \frac{R_{lay\,3}R_{lay\,4}}{R_{lay\,3} + R_{lay\,4}} = \frac{R_{lay\,5}R_{lay\,6}}{R_{lay\,5} + R_{lay\,6}}. \quad (19)$$

The copper loss of planar transformer P_{copper} can be estimated as follows:

$$P_{copper} = R_{pri}I_1^{\,2} + 2R_{sec}I_2^{\,2}, \quad (20)$$

where R_{pri} and R_{sec} are winding resistance of primary-side and secondary-side winding, respectively. I_1 and I_2 are root mean square (RMS) current of the primary-side and secondary-side winding.

Core loss of planar transformer P_{core} and total power loss P_{sum} can be derived as follows:

$$P_{core} = C_m f_s^{\,\alpha} B_m^{\,\beta} V_e,$$
$$P_{sum} = P_{copper} + P_{core}. \quad (21)$$

From these derived equations and FEM with Maxwell 3D, the relationship between primary-side winding width w_1 and P_{sum} can be obtained, as shown in Figure 13. The minimum total power loss can be found in this figure. From this figure, w_1 and air gap l_g can be decided. The ratio of a and b can be decided from Figure 14. It can be found that B_m is less than the limitation of B_m from Figure 15. From these figures and equations, the physical parameters of planar transformer can be obtained as follows: a = 5.15 mm, b = 3.7 mm, c = 16 mm, h = 2 mm, p = 4.3 mm, g = 0.5 mm, w_1 = 1.4 mm, w_2 = 3.3 mm, l_g = 1 mm, l_e = 20 mm, and A_e = 19.07 mm^2.

4. Experimental Results

Some experiments are done with parameters and components, as shown in Table 2. The prototype MHz-level LLC resonant DC-DC converter with GaN-HEMTs is shown in Figure 16. In this prototype circuit, to suppress the power loss at diodes and use the board area effectively, diodes D_1 and

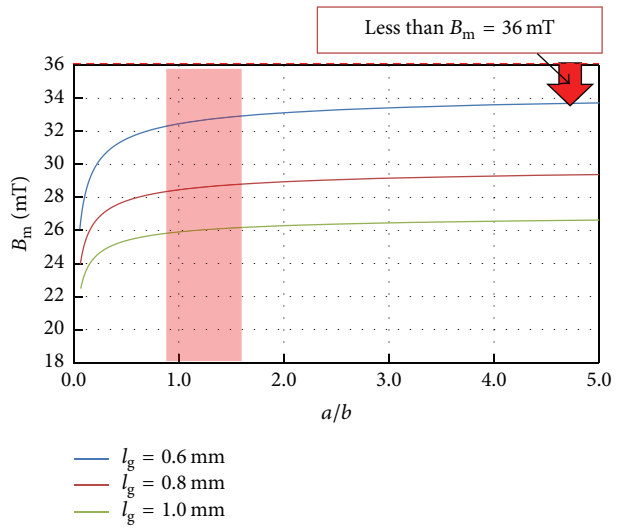

FIGURE 15: a/b versus B_m (fixed parameters: $L_{11} = 250$ nH, $\mu_s = 80$, $N_p = 3$, $\mu_0 = 4\pi \times 10^{-7}$ H/m, $h = 2$ mm, and $g = 0.5$ mm).

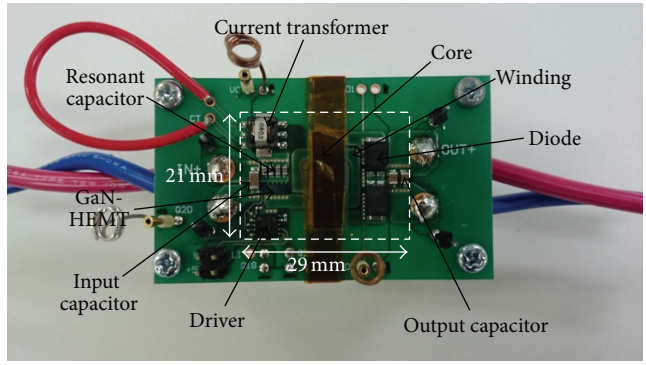

FIGURE 16: The prototype MHz-level isolated DC-DC converter with GaN-HEMTs.

TABLE 2: The parameters and components.

Name		Value
Primary-side GaN-HEMT (EPC2001C)	ON resistance: $R_{DS(ON)}$	7 mΩ
	Output capacitance: C_{oss}	430 pF (V_{DS} = 50 V)
	Reverse conduction voltage: V_{SD}	1.8 V
Secondary-side diode (PDS1040L)	Forward voltage: V_F	0.3 V
	Diode resistor: R_d	10 mΩ
	Junction capacitance: C_j	1 nF
Transformer (core: SY22)	Magnetizing inductance: L_m	195 nH
	Leakage inductance: L_{lk1}	40.82 nH
	Turns ratio: n	3
	Coupling coefficient: k	0.9095
Current transformer (B82801B)	Secondary-side short inductance: L_{CT}	7 nH
Resonant capacitor (C1608C0G2A152J)	Capacitance: C_{r1}, C_{r2}	6 nF
Driver (LM5113)		

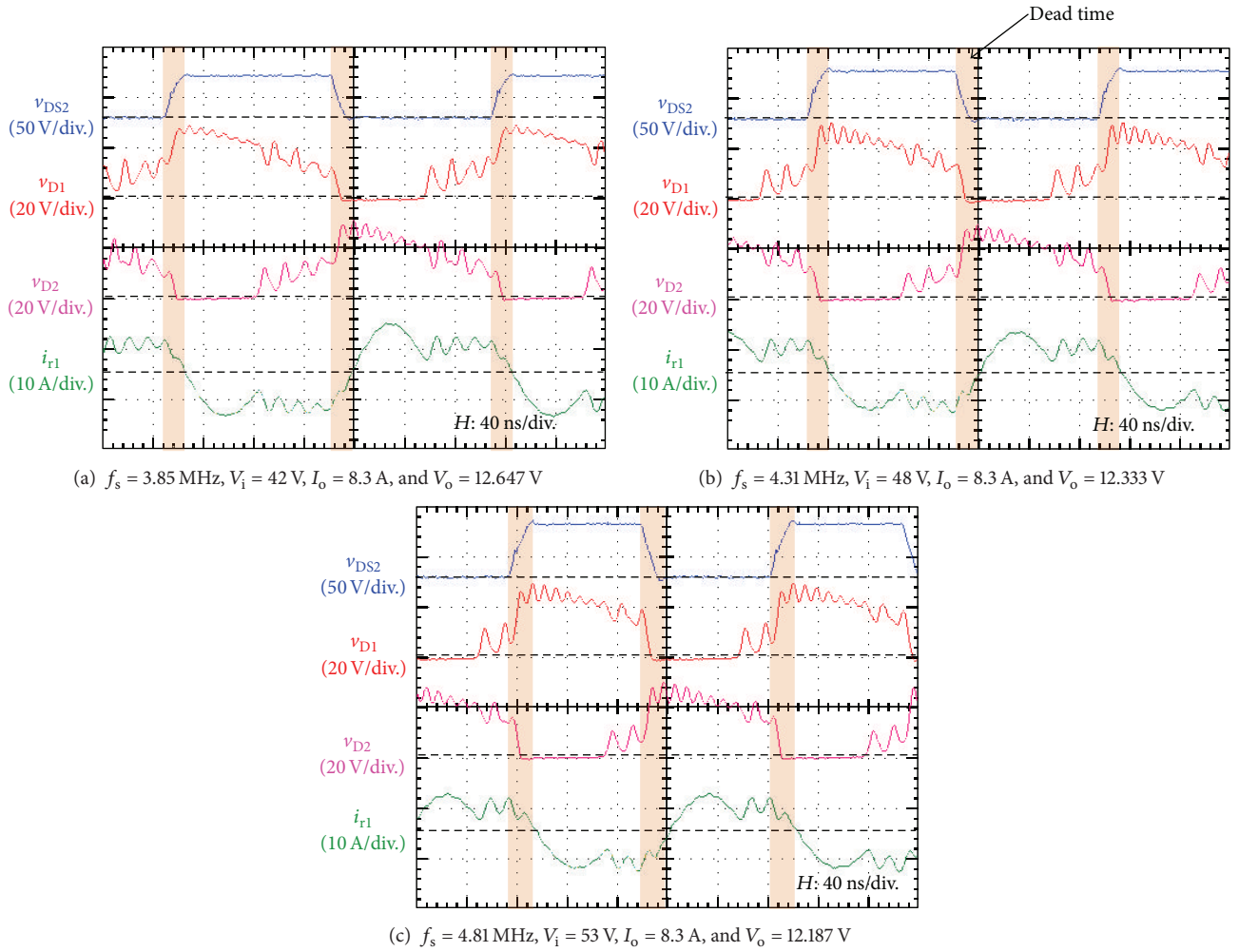

(a) f_s = 3.85 MHz, V_i = 42 V, I_o = 8.3 A, and V_o = 12.647 V

(b) f_s = 4.31 MHz, V_i = 48 V, I_o = 8.3 A, and V_o = 12.333 V

(c) f_s = 4.81 MHz, V_i = 53 V, I_o = 8.3 A, and V_o = 12.187 V

Figure 17: The voltage and current waveforms of each switch with various input voltages.

D_2 are 2 parallel connections, respectively. The volume of the prototype converter is 4.1 cm^3.

From Figure 17, the ZVS of the primary-side switches at turn-on seems to be achieved during the dead time even if the input voltage is changed. The temperature distributions of the prototype DC-DC converter are exhibited, as shown in Figure 18. Each core temperature can be found lower than 60°C. These results mean low flux density B_m. Each calculated B_m is as follows: B_m = 28.17 mT under V_i = 42 V and I_o = 8.3 A condition, B_m = 27.41 mT under V_i = 48 V and I_o = 8.3 A condition, and B_m = 26.90 mT under V_i = 53 V and I_o = 8.3 A condition. Also, at minimum input voltage, the temperature of winding and diode seems to be higher than other conditions.

From these experimental results and datasheets of devices [18, 19], each power loss analysis is conducted, as shown in Figure 19. It can be seen that the target efficiency is achieved at V_i = 48 and 53 V. On the other hand, it can be seen that the target efficiency is not achieved at worst condition V_i = 42 V. According to this analysis, the major reason of this problem is considered 6 W of copper loss.

Also, from these experimental results, it can be found that the power density of the prototype converter is 24.4 W/cc.

5. Conclusions

In this paper, the considerations of physical design and implementation for wide regulation range LLC resonant DC-DC converter with GaN-HEMTs are revealed. Also, the physical parameters and size of the planar transformer are optimized by using derived equations and FEM with Maxwell 3D.

The prototype LLC resonant DC-DC converter using GaN-HEMTs is tested with open loop. The specifications of this converter are that the input voltage is 42–53 V, the reference output voltage is 12 V, the load current is 8 A, the maximum switching frequency is about 5 MHz, and the total volume of the circuit is 4.1 cm^3. ZVS operation of the primary-side switches at turn-on can be achieved during the dead time even if the input voltage is changed. The prototype DC-DC converter is obtained more than 90% of power efficiency at V_i = 48 and 53 V, I_o = 8 A. Also, the power density of the prototype converter is 24.4 W/cc.

Competing Interests

The authors declare that they have no competing interests.

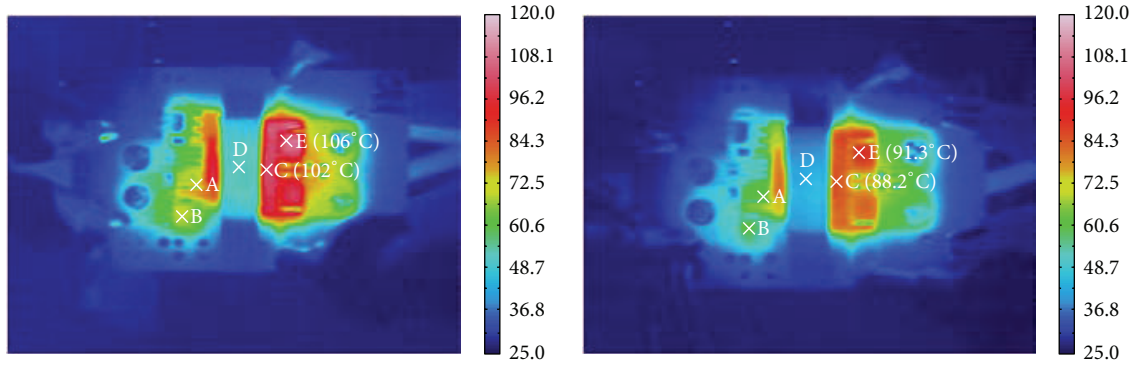

(a) f_s = 3.85 MHz, V_i = 42 V, I_o = 8.3 A, and V_o = 12.647 V

(b) f_s = 4.31 MHz, V_i = 48 V, I_o = 8.3 A, and V_o = 12.333 V

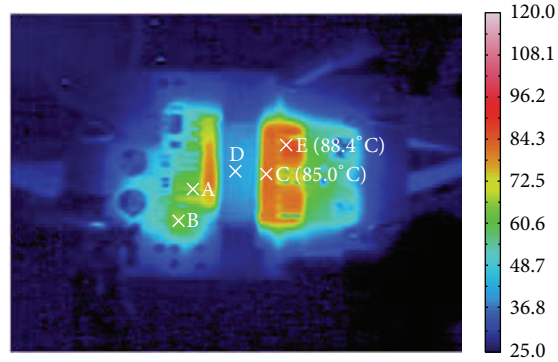

(c) f_s = 4.81 MHz, V_i = 53 V, I_o = 8.3 A, and V_o = 12.187 V

FIGURE 18: The temperature distributions (A: GaN, B: driver, C: winding, D: core, and E: diode).

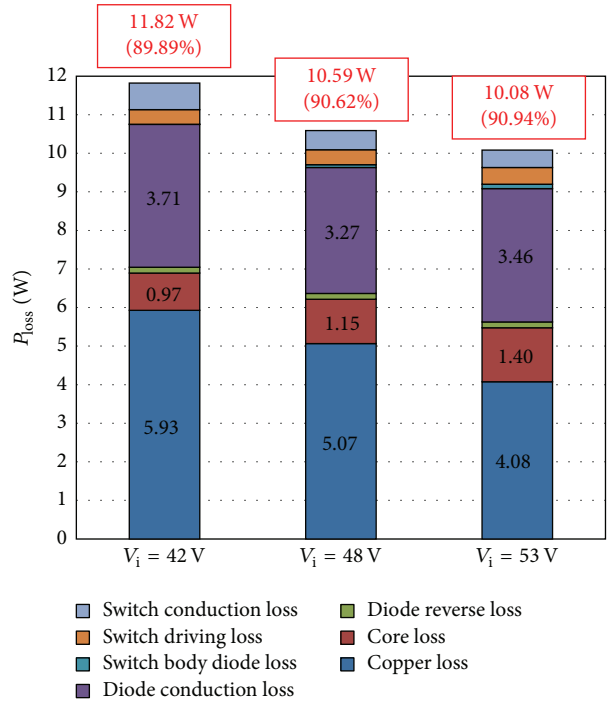

FIGURE 19: The power loss analysis of the experiment at P_o = 100 W.

References

[1] M. D. Seeman, S. R. Bahl, D. I. Anderson, and G. A. Shah, "Advantages of GaN in a high-voltage resonant LLC converter," in *Proceedings of the 29th Annual IEEE Applied Power Electronics Conference and Exposition (APEC '14)*, pp. 476–483, IEEE, Fort Worth, Tex, USA, March 2014.

[2] M. Tian, Y. Hao, K. Wang et al., "EMI modeling and experiment of a GaN based LLC half-bridge converter," in *Proceedings of the 9th International Conference on Power Electronics and ECCE Asia (ICPE-ECCE Asia)*, pp. 1961–1966, IEEE, Seoul, South Korea, June 2015.

[3] D. Reusch and J. Strydom, "Evaluation of gallium nitride transistors in high frequency resonant and soft-switching DC-DC Converters," *IEEE Transactions on Power Electronics*, vol. 30, no. 9, pp. 5151–5158, 2015.

[4] D. Reusch and J. Strydom, "Evaluation of gallium nitride transistors in high frequency resonant and soft-switching DC-DC Converters," *IEEE Transactions on Power Electronics*, vol. 30, no. 9, pp. 5151–5158, 2015.

[5] W. Zhang, Y. Long, Y. Cui et al., "Impact o f planar transformer winding capacitance on Si-based and GaN-based LLC resonant converter," in *Proceedings of the IEEE Applied Power Electronics Conference (APEC '13)*, pp. 1668–1674, March 2013.

[6] D. Reusch and F. C. Lee, "High frequency isolated bus converter with gallium nitride transistors and integrated transformer," in *Proceedings of the 4th Annual IEEE Energy Conversion Congress and Exposition (ECCE '12)*, pp. 3895–3902, Raleigh, NC, USA, September 2012.

[7] W. Zhang, F. Wang, D. J. Costinett, L. M. Tolbert, and B. J. Blalock, "Investigation of gallium nitride devices in high-frequency LLC resonant converters," *IEEE Transactions on Power Electronics*, vol. 32, no. 1, pp. 571–583, 2017.

[8] H. B. Kotte, R. Ambatipudi, and K. Bertilsson, "High-speed (MHz) series resonant converter (SRC) using multilayered coreless printed circuit board (PCB) step-down power transformer," *IEEE Transactions on Power Electronics*, vol. 28, no. 3, pp. 1253–1264, 2013.

[9] Z. Zhang, K. D. T. Ngo, and J. L. Nilles, "A 30-W flyback converter operating at 5 MHz," in *Proceedings of the 29th Annual IEEE Applied Power Electronics Conference and Exposition (APEC '14)*, pp. 1415–1421, Fort Worth, Tex, USA, March 2014.

[10] L. Cong and H. Lee, "A 110–250V 2MHz isolated DC-DC converter with integrated high-speed synchronous three-level gate drive," in *Proceedings of the IEEE Energy Conversion Congress and Exposition (ECCE '15)*, pp. 1479–1484, IEEE, Montreal, Canada, September 2015.

[11] H. B. Kotte, R. Ambatipudi, S. Haller, and K. Bertilsson, "A ZVS half bridge DC-DC Converter in MHz frequency region using novel hybrid power transformer," in *Proceedings of the International Exhibition and Conf. for Power Electronics, Intelligent Motion, Power Quality (PCIM '12)*, pp. 399–406, Nuremberg, Germany, May 2012.

[12] H. P. Park and J. H. Jung, "Design considerations of 1 MHz LLC resonant converter with GaN E-HEMT," in *Proceedings of the 17th European Conference on Power Electronics and Applications (EPE '15 ECCE-Europe)*, pp. 1–10, Geneva, Switzerland, 2015.

[13] H. de Groot, E. Janssen, R. Pagano, and K. Schetters, "Design of a 1-MHz LLC resonant converter based on a DSP-driven SOI half-bridge power MOS module," *IEEE Transactions on Power Electronics*, vol. 22, no. 6, pp. 2307–2320, 2007.

[14] K. Matsuura, H. Yanagi, S. Tomioka, and T. Ninomiya, "Power-density development of a 5MHz-switching DC-DC converter," in *Proceedings of the 27th Annual IEEE Applied Power Electronics Conference and Exposition (APEC '12)*, pp. 2326–2332, IEEE, Orlando, Fla, USA, February 2012.

[15] J. Millman and H. Taub, *Pulse, Digital and Switching Waveforms*, International Student, 1965.

[16] S. Yang, M. Shoyama, and S. Abe, "Design of low-profile LLC resonant converter for low transformer loss," in *Proceedings of the IEEE Region 10 Conference (TENCON '10)*, pp. 1301–1306, Fukuoka, Japan, November 2010.

[17] B. Lu, W. Liu, Y. Liang, F. C. Lee, and J. D. Van Wyk, "Optimal design methodology for LLC resonant converter," in *Proceedings of the 21st Annual IEEE Applied Power Electronics Conference and Exposition (APEC '06)*, pp. 533–538, March 2006.

[18] NiZn Material Characteristics, TDK, 2014, https://product.tdk.com/info/en/catalog/datasheets/ferrite_ni-zn_material_characteristics_en.pdf.

[19] eGaN FET Datasheet: EPC2001C—Enhancement Mode Power Transistor, http://epc-co.com/epc/Portals/0/epc/documents/datasheets/EPC2001C_datasheet.pdf.